

Human bone material characterization: integrated imaging surface investigation of male fragility fractures

R. Zoehrer · E. Perilli · J. S. Kuliwaba · J. G. Shapter ·
N. L. Fazzalari · N. H. Voelcker

Received: 2 February 2011 / Accepted: 27 May 2011 / Published online: 22 June 2011
© International Osteoporosis Foundation and National Osteoporosis Foundation 2011

Abstract

Summary The interrelation of calcium and phosphorus was evaluated as a function of bone material quality in femoral heads from male fragility fracture patients via surface analytical imaging as well as scanning microscopy techniques. A link between fragility fractures and increased calcium to phosphorus ratio was observed despite normal mineralization density distribution.

Introduction Bone fragility in men has been recently recognized as a public health issue, but little attention has been devoted to bone material quality and the possible efficacy in fracture risk prevention. Clinical routine fracture risk estimations do not consider the quality of the mineralized matrix and the critical role played by the different chemical components that are present. This study uses a combination of different imaging and analytical techniques to gain insights into both the spatial distribution and the relationship of phosphorus and calcium in bone.

Methods X-ray photoelectron spectroscopy and time-of-flight secondary ion mass spectrometry imaging techniques were used to investigate the relationship between calcium and phosphorus in un-embedded human femoral head specimens from fragility fracture patients and non-fracture age-matched controls. The inclusion of the bone mineral density distribution via backscattered scanning electron microscopy provides information about the mineralization status between the groups.

Results A link between fragility fracture and increased calcium and decreased phosphorus in the femoral head was observed despite normal mineralization density distribution. Results exhibited significantly increased calcium to phosphorus ratio in the fragility fracture group, whereas the non-fracture control group ratio was in agreement with the literature value of 1.66 M ratio in mature bone.

Conclusions Our results highlight the potential importance of the relationship between calcium and phosphorus, especially in areas of new bone formation, when estimating fracture risk of the femoral head. The determination of calcium and phosphorus fractions in bone mineral density measurements may hold the key to better fracture risk assessment as well as more targeted therapies.

R. Zoehrer · J. G. Shapter · N. H. Voelcker (✉)
School of Chemical and Physical Sciences, Flinders University,
GPO Box 2100, Bedford Park,
Adelaide, SA 5042, Australia
e-mail: Nico.voelcker@flinders.edu.au

E. Perilli · J. S. Kuliwaba · N. L. Fazzalari
Bone and Joint Research Laboratory, Surgical Pathology,
SA Pathology and Hanson Institute,
Frome Road,
Adelaide, SA 5000, Australia

E. Perilli · J. S. Kuliwaba · N. L. Fazzalari
Discipline of Anatomy and Pathology,
The University of Adelaide,
Frome Road,
Adelaide, SA 5005, Australia

Keywords Backscattered scanning electron microscopy · Bone mineral density distribution · Calcium/phosphorus ratio · Male fragility fractures · Time-of-flight secondary ion mass spectrometry · X-ray photoelectron spectroscopy

Introduction

Osteoporosis is characterized by a systemic impairment of bone mass, strength and microarchitecture, which increases

the propensity of fragility fractures [1]. Studies of osteoporosis and bone fragility over the last decade have focused on pathogenesis, diagnosis and treatment in women. However, recent epidemiological studies have shown that osteoporosis in men is an increasingly important clinical issue. Although osteoporosis and related fractures are less frequent in men, still ~25% occur in men [2]. The diagnosis, however, is less well recognized in men because the World Health Organization's definition of osteoporosis has been established for postmenopausal women of Caucasian ethnicity. The diagnosis, based on densitometric measurement of bone mineral density (BMD), defined by a sex-specific T-score < -2.5, only identifies half of the future fractures that will occur in postmenopausal women [3] and this predictive value is even smaller in men [4]. Because bone loss occurs insidiously and is initially asymptomatic, osteoporosis is often only diagnosed after the first clinical fracture has occurred as applicable for the specimens analyzed in this study [1]. The degree and distribution of bone mineralization are known contributors to the stiffness and hardness of the bone material [5], which can be measured by backscattered electron imaging (BSEM) as bone mineral density distribution (BMDD) [6]. It is also known that mineral characteristics alone do not satisfactorily predict future fracture risk [7]. Therefore, the concept of bone quality was defined as the sum of all factors mediating bone mechanical properties at constant bone mass, describing a set of characteristics that influence bone strength [8].

The effect of calcium (Ca) and phosphorus (P), as the main elements of the bone mineral building block hydroxyapatite (HA) ($\text{Ca}_5(\text{PO}_4)_3(\text{OH})$), are especially interesting when reviewing the effects of nutrient intake of Ca and P on bone tissue. Sufficient amounts of Ca and P are needed not only to support mineralization of bone tissue but also to suppress excessive and persistent elevations of circulating parathormone, hypothesized as a potential mechanism responsible for low bone mass [9]. Most studies on P have focused on the effect of high P intakes on Ca balance and bone metabolism. The present study addressed whether an imbalance in Ca and P and its distribution in the bone tissue is different between fragility fracture and non-fracture subjects, suggesting they may have a role in determining bone quality. Consequently, determination of the Ca/P ratio and the BMDD may provide an additional measure of bone mineral changes and may add to our understanding of the material quality changes occurring in bone diseases resulting in fragility fractures. The measurements of mineral changes, especially Ca/P tissue measurements typically do not refer to the intact bone [7]. There is a clear need for the application of analytical techniques capable of providing spectral information on Ca and P levels and the spatial distributions in bone. Technically, *in vivo* measurements of

the Ca/P ratio are possible by using enhanced synchrotron radiation microtomography systems [10]. Such investigations have been successfully performed in ovariectomized rats [11].

Time-of-flight secondary ion mass spectrometry (TOF-SIMS) is a routine analytical tool for the characterization of materials, particularly material surfaces [12, 13], and imaging TOF-SIMS is widely used in the biomaterials community to study biomaterial–protein interactions and implant tissue interactions [14] providing detailed chemical structure information with very high sensitivity and an ultimate spatial resolution in the order of 100 nm.

X-ray photoelectron spectroscopy (XPS) complements and validates TOF-SIMS analysis by allowing the determination of surface elemental composition with a spatial resolution of 3 μm , and it has recently been used in the study of bone formation in bone implant materials [15]. The application of such methods for bone quality research is an exciting prospect due to the high information content that these analytical methods afford. We also noticed a conspicuous lack of data in the literature in terms of bone material quality and analysis of Ca and P of male subjects sustaining fragility fractures. The aim of this study was to estimate and image the Ca/P ratio for intact trabecular bone of the femoral head to study regions most likely contributing to reduced bone strength. Therefore, we measured and imaged Ca and P in male patients using TOF-SIMS and XPS to investigate whether the specimens from fragility fracture patients (FF) show altered Ca and P levels at the nanoscale compared to a non-fracture control (CTL) group.

Materials and methods

Study groups

Patients chosen were based on clinical reports upon hospitalization for which research ethics committee approval was given, and all subjects gave written informed consent. Factors excluded were hypertension, dementia, diabetes mellitus, coronary heart disease, chronic obstructive pulmonary disease, malignant disease or specific bone diseases and anti-resorptive, anabolic or hormonal therapy. None of the patients were treated for conditions related to rickets, hypoparathyroidism and hyperphosphatemia and hyper- and hypoparathyroidism. The age range was between 65 and 80 years (five FF and four CTL, Table 1). Bone segments of the superior part of the femoral head (Fig. 1) from a CTL group, obtained from post-mortem cases, were analyzed and compared with age-matched specimens from a male FF group that had undergone hip arthroplasty surgery for a non-traumatic

Table 1 Summary of subject information

	Age (years)	Comorbidities/cause of death	Drugs	Mobility	Prior surgery
Fragility fractures	68	No information	Aspirin	Walks unaided	Hernia repair cataracts
	79	Chronic obstructive airways disease, Parkinson's disease	Paracetamol, ventolin, atrovent	Unknown	Cataracts
	72	Angina, gastroesophageal reflux disease	Isosorbide, omeprazole, temazepam, perhexiline	Walks with frame	Nephrectomy
	80	Bowel obstruction, Alzheimer's disease	Paracetamol, donepezil, nitrazepam	Walks with frame	Unknown
	80	Bowel obstruction	Donepezil, methadone, nitrazepam	Walks with frame	Lumbar fusion bladder operation
Controls	80	Sepsis, respiratory failure	Unknown	Unknown	Unknown
	65	Myocardial infact	Unknown	Unknown	Unknown
	73	Cerebrovascular disease	Unknown	Unknown	Unknown
	72	Chronic renal failure	Unknown	Unknown	Unknown

subcapital femoral fracture. The femoral head was cut with a low speed bone-cutting diamond saw (Buehler, Isomet, Hong Kong, China) under constant irrigation (50% ethanol) throughout the study. Specimens were polished with ascending grades of sandpaper (6,000 and 8,000 grit) followed by a final dry polishing step (12,000 grit) removing the outermost layer of the surface until they appeared flat and without scratches under a light microscope. Specimens underwent a series of washes with analytical reagent grade ethanol, acetone and hexane, to reduce contaminations, dried and de-gassed for at least 1 week. To ensure that the Ca and P ion surface properties were not affected by part dissolution of mineral due to a possible equilibrium in the irrigation medium during preparation, we performed one dry polishing step (12,000 grit) between measurements on one specimen. Differences in distribution between the elements P and Ca before and after dry polishing were $p > 0.105$ and $p > 0.485$, respectively for TOF-SIMS and $p > 0.099$ and $p > 0.503$, respectively for XPS. Methods are listed in chronological order as the experiments were performed.

Area selection criteria

Area selection was performed on un-embedded and un-coated specimens on a low-resolution benchtop SEM (FEI Phenom, Oregon, USA), equipped with a backscattered scanning electron (BSE) detector and operating with an accelerating voltage of 5 keV, from now on referred to as BSE-FEI. Bone matrix mineralization is known to vary over microscopic regions, with the age of the bone structural units (BSUs), the recently deposited BSUs being less calcified than the older ones as indicated by darker grey regions in the electron microscopy images (Fig. 1). The process of mineralization consists of a slow and gradual

maturation of the bone mineral component and is characterized by different grey levels in the BSEM images [16]. To compare differences between primary (darker areas) and secondary (lighter areas) mineralization, we selected three different areas of interest per specimen at the BSU level based on the following morphological criteria: The more recently formed bone, which is undergoing primary mineralization, is found at the surface of bone trabeculae, whereas the highly mineralized regions of secondary mineralization usually correspond to interstitial bone [17, 18]. This study design enables the analysis of representative regions of the bone surface exposed by sectioning of the femoral bone specimens. Given that bone is a heterogeneous material, the sectioning of the bone has enabled the analysis of a statistically representative volume sample of the femoral bone being studied. Examples for area selection obtained via BSE-FEI for the proposed investigations can be seen in Fig. 1, *D1–D5*.

X-ray photoelectron spectroscopy

Imaging and spectral analyses were performed using an AXIS Ultra DLD spectrometer (Kratos Analytical, Manchester, UK) with a Mg(K α) source of energy 1,253.6 eV (15 mA, 14 kV). Additional spectral analyses were performed using a Phoibos 100 analyser from SPECS (X-ray source from SPECS XR 50, Surface Nano Analysis GmbH, Berlin, DE) on a custom-built apparatus. Changes in the atomic percentages of Ca and P were analyzed by XPS survey spectra. The specimens were mounted on standard sample stubs using double-sided carbon tape. A charge neutralizer system was used on all specimens. The total pressure in the system during analysis was 6×10^{-9} Torr. Data were obtained from three separate areas on each sample based on the area selection

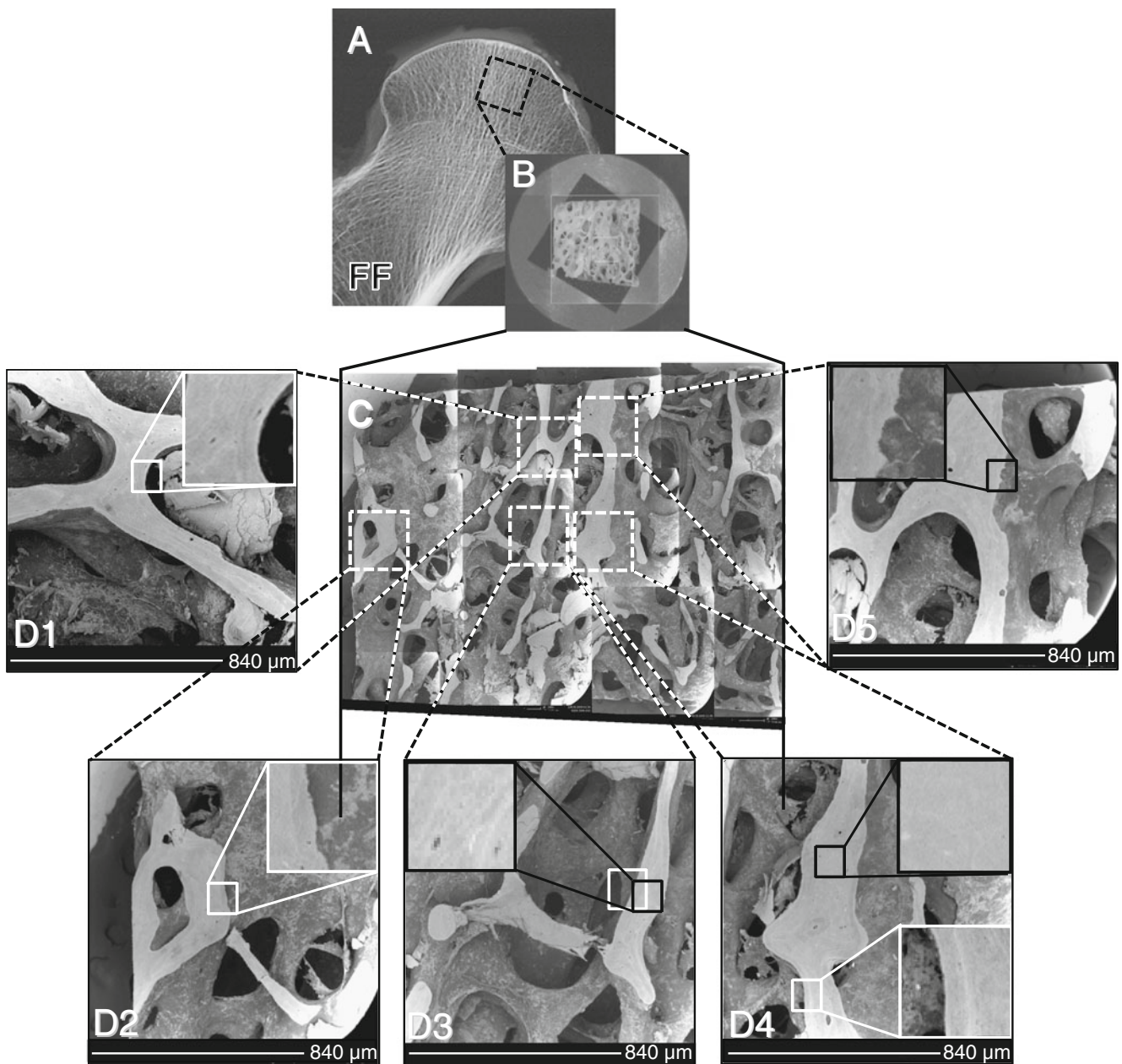


Fig. 1 Area selection via BSEM-FEI. **a** Representative femoral head region for bone specimen preparation from a fragility fracture patient (FF). **(b)** Overview photograph and **(c)** montage BSEM-FEI image.

D1–D5 Single BSEM-FEI images (1–5) for area selection [CaLOW (white box): *D1, D2, D4*; CaHIGH (black box): *D3, D4, D5*]

via BSE-FEI as described earlier on un-embedded and un-coated specimen. To obtain binding energies for the high-resolution imaging as well as for calibration purposes, high-resolution spectra were obtained for each element separately [Ca, P and carbon (C), lens mode; hybrid, pass energy 20, 0.1 eV steps, three sweeps]. The binding energy in the XPS spectra was corrected with respect to the C 1 s peak attributable to aliphatic carbon at 284.6 eV. Additional survey spectra of two more subjects were recorded to be able to compare atomic percentage

values for Ca and P from different patients and different areas within the same group (AXIS ultra, lens mode; survey, centred at 550 eV, width of 1,100 eV, 0.5 eV steps, 55 ms dwell time, total of 15 sweeps, SPECS, 0 to 600 eV, 0.5 eV steps, 50 ms dwell time, total of 25 min acquisition time). High-resolution images for Ca and P with an instrumental maximum analysis area of $200 \times 200 \mu\text{m}^2$ and a spatial resolution of $3 \mu\text{m}$ were performed with the AXIS system. XPS high-resolution images were obtained from one sample per group (FF vs. CTL) acquired on three

different areas (described earlier). Single images for each area were overlaid to show differences or correlations in the distribution of Ca and P as a function of spatial pattern. The elemental composition of the high-resolution spectra were recorded at an emission angle normal to the surface using a pass energy of 40 eV and an integration time of 1,200 s, yielding a typical peak width of about 0.5 eV. From each high-resolution Ca image, one area representing high levels of Ca (CaHIGH) and one area representing low levels of Ca (CaLOW) were chosen for small spot spectroscopy to obtain survey spectra (lens mode, small spot, pass energy 80, centred at 550 eV, width of 1,100 eV, 0.5 eV steps, total of 15 sweeps). Data processing was carried out using CasaXPS software (version 2.3.14) using Shirley background and Gaussian/Lorentzian peak shapes [19].

Time-of-flight secondary ion mass spectrometry

TOF-SIMS experiments were performed on un-embedded and un-coated surfaces using a static Physical Electronics Inc. PHI TRIFT V nanoTOF instrument equipped with a pulsed liquid metal ^{79+}Au primary ion gun. The gun was operated at 30 kV energy in an unbunched mode to optimize spatial resolution. Raw spectra were collected in positive SIMS modes, typically using a raster area of $500 \times 500 \mu\text{m}^2$ and a spatial resolution of 120 nm. A pulsed electron gun was used for charge compensation. TOF-SIMS spectra in the m/z 0–600 range were acquired from every position within the raster. TOF-SIMS raw data were calibrated using WincadenceN software (Physical Electronics Inc.). The calculation of the peak intensities in counts per element for Ca and P was performed using the WincadenceN software analysis tool. The exact same areas of un-embedded and un-coated specimen ($n=3$ per group) as investigated via XPS were measured as well as additional specimen (CTL $n=4$; FF $n=5$). The mass spectra and the corresponding images were then used to determine the composition and distribution of sample surface constituents of Ca (m/z 39.9) and P (m/z 30.9). From the acquired images, line scans over the areas of CaLOW and CaHIGH were performed. Area selection for the line scans was based firstly on the highest amount of Ca present within one specimen [(Fig. 2c, f: indicated by 2) CaHIGH, as for the XPS measurement] and secondly, based on areas starting at the endosteal surface of the trabecular bone, towards the inner quiescent area [(Fig. 2c, f: indicated by 1) CaLOW]. The investigated areas of CaHIGH and CaLOW were expressed as measures of distance of the bone, characterizing the heterogeneity of the Ca and P values. The intensities of P (m/z 30.9) and Ca (m/z 39.9) were normalized to the total ion count to give the normalized ion count (NIC) [20].

Backscattered scanning electron microscopy

Specimens were processed using standard protocols for resin embedding as described earlier for BSEM measurements [21, 22]. The bone specimens were analyzed using a Philips XL20 scanning SEM with a tungsten filament at 15 kV, working distance of 15 mm and a two-sector backscattered electron detector. The surface of each bone specimen was carbon coated. The intensity of the backscattered electrons, and thus the grey levels in the resulting backscattered images, is proportional to weight concentration of the calcium in the bone. The BSEM protocol and the carbon/aluminum standard (spectrographically pure carbon, Bal-Tec, Liechtenstein/Specpure aluminum, Johnson Matthey Chemicals, London) calibration were based on the validated method described by Roschger et al. [23, 24]. Images were taken from ten different trabecular regions per sample at a magnification of $\times 200$, and the data were pooled to produce a mean Ca weight percent content by analyzing the images using Matlab image processing software (Mathworks Inc. Natick, USA). The mean Ca content was obtained for each individual and the data were pooled to produce a distribution for the control and fragility fracture groups.

Statistical analysis

Differences in measurements were analyzed using Mann–Whitney non-parametric tests for comparisons among the two study groups, and $p < 0.05$ was considered statistically significant. Results were expressed as means and standard deviation in Table 2 and as means and standard error of the mean in the results and Figs. 3, 4 and 5.

Results

XPS

High-resolution imaging

The distribution of Ca (red) at the endosteal surface region of the trabecular spicule presented distinctive differences within one BSU [Fig. 2b (CTL), e (FF), white arrow]. Ca appeared to be distributed with very little involvement of P (green) at this outer surface of trabecular spicules in the FF group, whereas in the CTL group, P was present more frequently. In the images of the FF group, this Ca distribution was around $25 \mu\text{m}$ in width, whereas that of the CTL group was only around $50 \mu\text{m}$ in diameter measured from the edge towards the inside of the trabecular spicules (Fig. 2b, e, white arrow). The yellow areas in the

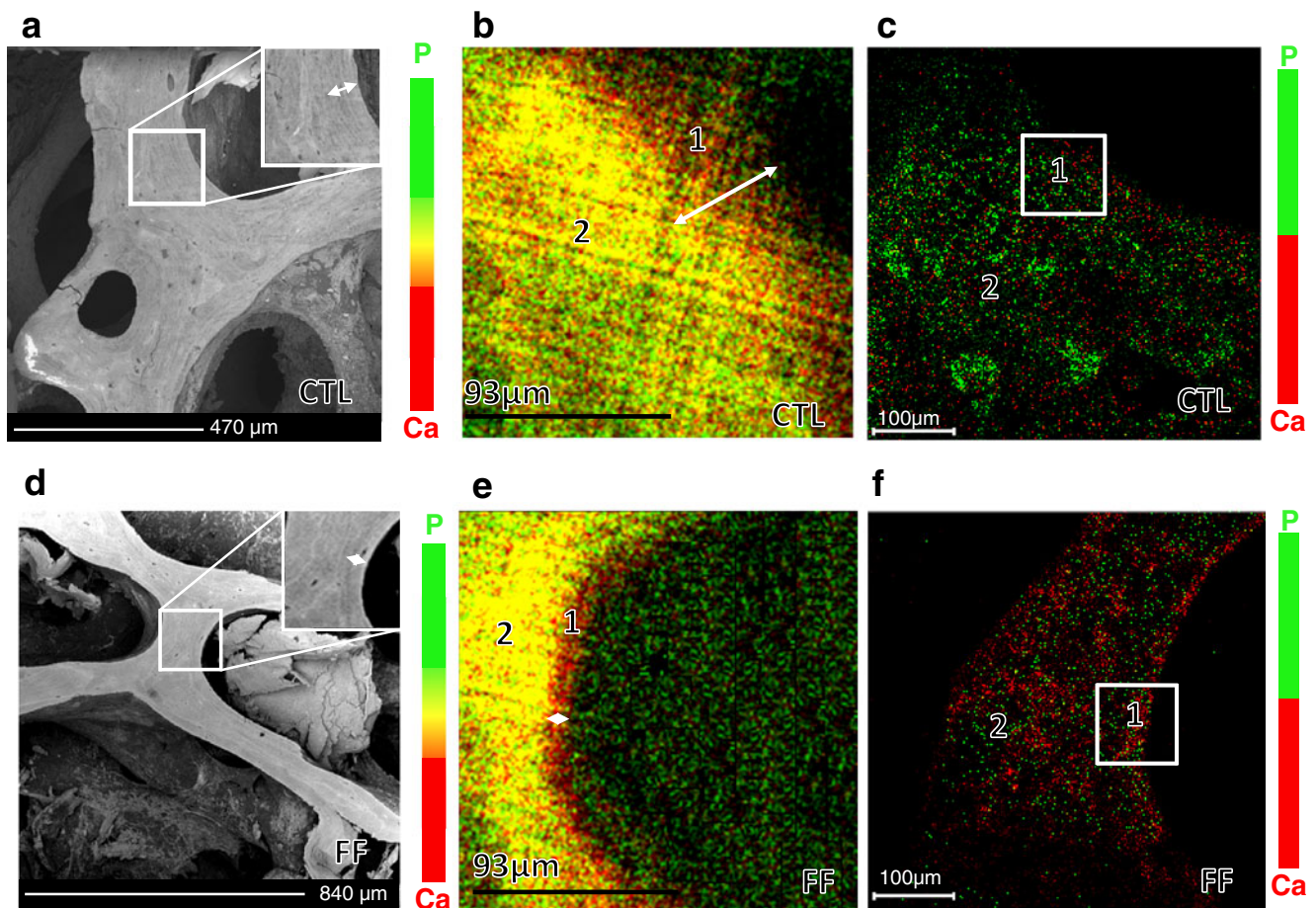


Fig. 2 Images of BSEM, XPS and TOF-SIMS. **a, d** Overview BSEM-FEI image obtained for area selection. **b, e** XPS high-resolution image overlay of Ca (red) and P (green; yellow equals P:Ca; $200 \times 200 \mu\text{m}^2$). **1** CaLOW and **2** indicate areas for small spot spectroscopy and *arrows* indicate BSU. **c, f** TOF-SIMS image overlay

of Ca (red) and P (green; $500 \times 500 \mu\text{m}^2$). Line scan data analysis is indicated by **(1)** CaLOW and **(2)** CaHIGH. *Arrows* show BSUs. *White box* in **a, c, d** and **f** show the measurement area of $200 \times 200 \mu\text{m}^2$ used in XPS

images represent an equal proportion of Ca and P (1:1). These areas appear in the FF group less evenly distributed than in the CTL group. The images from the FF specimens infrequently showed patches of low levels of Ca and high levels of P in contrast to the images acquired from the CTL specimens.

Small spot spectroscopy

Based on the XPS high-resolution Ca images, small spot spectroscopy was performed on areas indicating lower levels of Ca by means of high-resolution XPS imaging (CaLOW), (Fig. 2b, e, indicated by 1) as well as on areas characterized by high levels of Ca (CaHIGH), (Fig. 2b, e, indicated by 2). The calculated atomic percentage for Ca in the areas of CaLOW and CaHIGH exhibited no significant difference within the FF group but a statistically significantly increased Ca value within the CTL

group (Fig. 3a, Table 2). A significant increase in Ca atomic percentage for CaLOW was observed in the FF group compared to the CTL group ($p=0.036$) (Fig. 3a, Table 2). Ca atomic percentage in CaHIGH areas did not exhibit statistically significant differences ($p=0.445$). The most conspicuous difference between the CTL and the FF groups was observed in the results for P atomic percentage (Fig. 3b), where P content was almost 40% lower in the FF group in both areas when compared to CTL group ($p < 0.0001$, $p=0.002$). The calculated P content in atomic percentage was significantly lower in CaLOW areas when compared to CaHIGH areas in the FF group ($p=0.015$), as well as in the CTL group ($p=0.038$) (Fig. 3b). The resulting Ca/P ratio exhibited a significant increase in CaHIGH areas (1.68 ± 0.20 vs. 2.89 ± 0.42 ; $p=0.026$) and an even higher significant increase in CaLOW areas in the FF group when compared to the CTL group [1.16 ± 0.05 vs. 2.96 ± 0.11 ; $p < 0.0001$ (Fig. 3c)].

Table 2 Summary of TOF-SIMS, XPS and BSEM results

		At. % of Ca				At. % of P				
		Avg±SD	p value	CV%	Min, max	Avg±SD	p value	CV%	Min, max	
XPS	CaLOW	CTL	5.55±0.38	0.04	6.0	5.11, 5.77	4.91±0.64	<0.0001	10.5	3.78, 5.95
		FF	7.58±0.49		1.4	6.72, 7.86	2.63±0.50		2.9	2.20, 4.24
	CaHIGH	CTL	9.05±2.23	0.45	4.5	6.15, 12.18	5.44±1.08	0.002	17.5	3.54, 6.01
		FF	9.15±4.13		15.5	3.79, 16.60	3.34±0.84		18.4	2.74, 4.43
TOF-SIMS	CaNIC	CTL	0.510±0.020	0.35	8.4	0.11, 0.61	0.012±0.007	<0.0001	10.4	0.006, 0.021
		FF	0.540±0.030		13.1	0.01, 0.79	0.007±0.005		34.8	0.001, 0.013
	wt. % Ca	CTL	20.84±0.96	0.18	1.74	8.86, 32.80	5.83±0.25	0.10	4.25	5.55, 6.01
		FF	22.64±0.92		1.40	11.75, 34.02	4.20±0.20		4.82	3.97, 4.35

Results are expressed as mean±SD, CV%, min, max values and p value between CTL and FF

XPS X-ray photoelectron spectroscopy, BSEM backscattered scanning electron microscopy, FF fragility fracture patients, CTL non-fracture control group, FWHM full width at half maximum, PNIC phosphorous normalized ion count, CaNIC calcium normalized ion count, TOF-SIMS time-of-flight secondary ion mass spectrometry, CaLOW low levels of Ca, CaHIGH high levels of Ca

Additional survey scans

To increase the statistical representative volume of specimen, survey scans of two additional specimen and three additional

areas of interest were selected based on low-resolution BSE-FEI images. The FF group showed a higher mean Ca value (8.55±0.40 at.%) compared to the CTL group (7.99±0.24 at.%), although not reaching statistical significance

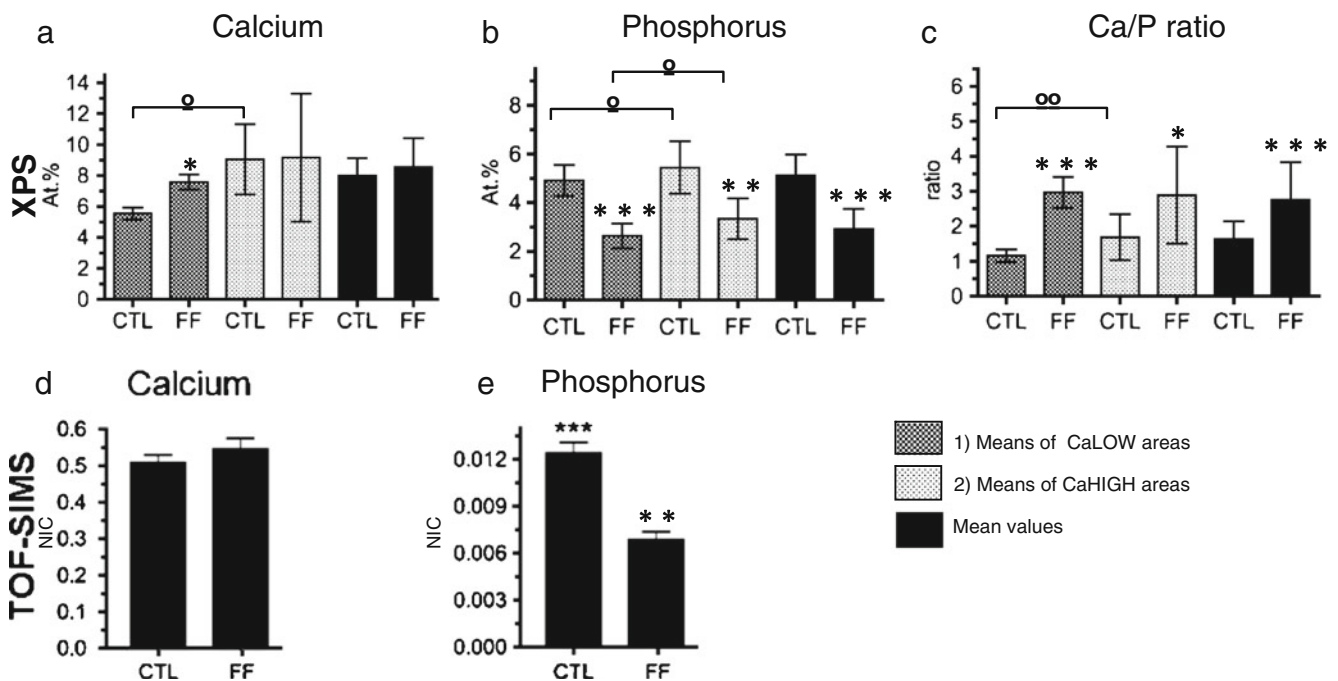


Fig. 3 Comparisons of XPS and TOF-SIMS measurements. **a, d** Atomic percentage of Ca for CTL and FF, **(b, e)** atomic percentage of P for CTL and FF and **(c)** XPS-derived Ca/P ratio for CTL and FF. Results are displayed in *light grey bars* (1) CaLOW and in *dark grey bars* (2) CaHIGH. *Black columns* represent average values of three

areas of different specimens per group (XPS n=6; TOF-SIMS n=9). Graphs are presented as mean±SE. Significance of differences within groups between areas (CaLOW vs. CaHIGH) are indicated as °p<0.05, °°p<0.01. Significance of differences between FF and CTL group are indicated as *p<0.05; **p<0.01, ***p<0.001

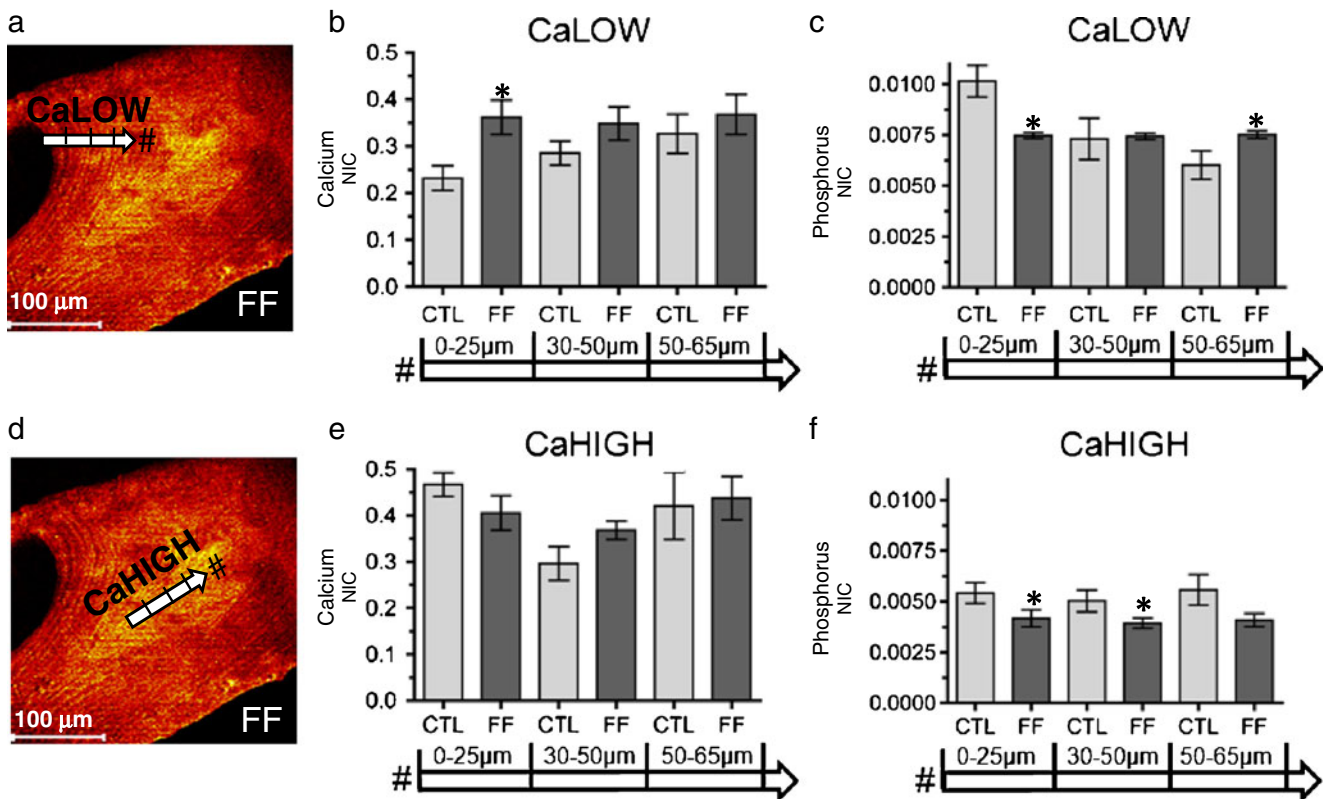


Fig. 4 TOF-SIMS line scan results. Image of FF specimen showing representative areas of (a) CaLOW and (d) CaHIGH line scan measurements (0–65 μm). b, e Ca ion counts (CTL $n=4$; FF $n=5$), (c, f) P ion counts. Line scan ion count results for Ca and P over a total of 65 μm

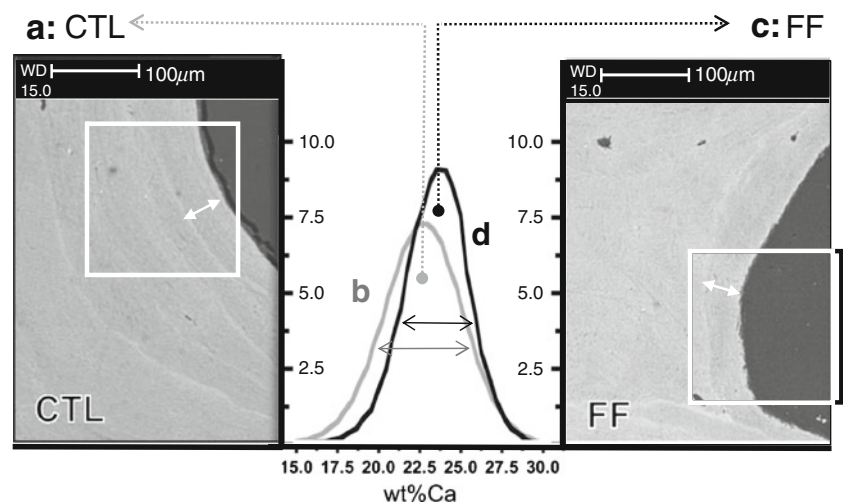
reaching from the endosteal site of the trabecular bone into the centre of the surface were subdivided into results for 0–25, 30–50 and 50–65 μm. Three different measurements of CaLOW and CaHIGH per specimen were analyzed. Arrow on image is not in scale

($p=0.12$) (Fig. 3a, black bars). The group mean P atomic percentage value was ~50% lower in the FF group when compared to the CTL group (2.97 ± 0.19 at.% vs. 5.12 ± 0.18 at.%; $p<0.0001$) (Fig. 3b, black bars). The resulting mean Ca/P ratio was significantly increased in the FF group compared to the CTL group (2.75 ± 0.23 vs. 1.63 ± 0.11 ; $p<0.003$) as shown in Fig. 3c (black bars).

TOF-SIMS

TOF-SIMS was performed for the same sample areas investigated by XPS as well on additional specimen to increase the statistically representative number (two for the FF group (total $n=5$) and one for the CTL group (total $n=4$). Atomic percentages are not obtained by TOF-

Fig. 5 BSEM results. Zoom in ($\times 500$) BSEM image of (a) one subject of the CTL group, 80 years of age, and (c) one subject of the FF group, 72 years of age. (b) CTL and (d) FF corresponding BMDD curves, arrows indicate FWHM. The area in a, c marked with a white box corresponds to the area investigated by XPS ($200\times 200\ \mu\text{m}^2$) with arrows indicating bone areas of distinct lower weight percent Ca. Curves represent pooled weight percent Ca representing the BMDD for three CTL and three FF specimens



SIMS. Instead, NIC for Ca and P are measured and compared [22].

Imaging

The patches of high P ion peak intensity could be observed in TOF-SIMS images (Fig. 2c, f). The FF group showed a greater frequency of areas of high Ca ion intensity when compared to the CTL group. The distribution of the Ca ions on the endosteal surface of the trabecular bone was consistent with what was observed in the XPS images of the same BSU investigated. In the FF group, the line of Ca ions at the endosteal surface of the BSU appeared distinct and only a few microns in width (~25 μm), whereas in the CTL group, the Ca was distributed more diffusely over a larger area within the BSU (~50 μm). Based on the acquired ion maps, line scans from these images were acquired to afford information about Ca and P NIC as a function of tissue area. The aim was to analyze areas of different tissue age to compare areas of lower, primary mineralization with areas of higher, secondary mineralization.

Line scans

The NIC for Ca and P as a function of distance from the endosteal site into the centre of the surface are plotted in Fig. 4a–c (CaLOW) and d–e (CaHIGH). Figure 4a, d shows a representative TOF-SIMS total ion image of an FF patient, and representative areas chosen for CaLOW and CaHIGH line scan investigations are indicated by arrows.

CaLOW The FF group exhibited significantly higher mean Ca NIC when compared to CTL in the CaLOW areas (0.282 ± 0.018 NIC vs. 0.364 ± 0.024 NIC, $p=0.0144$) (data not shown). A statistically significant increase in Ca NIC was found when comparing the NIC in the first 25 μm of the BSU of the FF group with the CTL group (0.362 ± 0.036 NIC and 0.232 ± 0.026 NIC, respectively, $p=0.015$). No significant difference between the FF and the CTL group in the signal for Ca after a distance of 30 μm up to 50 μm was observed (0.348 ± 0.024 NIC vs. 0.285 ± 0.025 NIC, $p=0.218$). The measurements in Ca after 50 μm were not significantly different between the groups (0.368 ± 0.042 NIC, 0.364 ± 0.040 NIC, $p=0.801$) (Fig. 4b). The mean P signal in the CaLOW areas was not significantly different between the FF and the CTL group (0.008 ± 0.001 NIC vs. 0.008 ± 0.001 NIC, $p=0.206$) (data not shown). The P NIC were significantly lower in the FF group compared to the CTL over the first 25 μm of the BSU (0.007 ± 0.001 NIC, 0.010 ± 0.001 NIC, $p=0.022$), whereas after 25 μm , no significant difference was observed between CTL and FF (0.007 ± 0.001 NIC, 0.007 ± 0.001 NIC, $p=0.306$). Surpris-

ingly, a significant increase of P signals in the FF group after 50 μm up to 65 μm was observed in comparison to the CTL group (0.008 ± 0.001 NIC, 0.006 ± 0.001 NIC, $p=0.021$) (Fig. 4c).

CaHIGH No significant differences in Ca NIC between the FF group and the CTL group in areas of CaHIGH were observed (0.343 ± 0.014 NIC vs. 0.362 ± 0.022 NIC, $p=0.653$) (data not shown). No significant differences in Ca signals as a function of distance were observed (0–25 μm , 0.483 ± 0.039 NIC vs. 0.450 ± 0.025 NIC, $p=0.738$; 30–50 μm , 0.434 ± 0.047 NIC vs. 0.361 ± 0.021 NIC, $p=0.170$; 50–65 μm , 0.468 ± 0.048 NIC vs. 0.374 ± 0.064 NIC, $p=0.139$) (Fig. 4e). The mean P NIC in the CaHIGH areas was significantly lower in the FF group when compared to the CTL group (0.004 ± 0.001 NIC vs. 0.006 ± 0.001 NIC, $p<0.001$) (data not shown). The NIC for P exhibited a significant decrease in the FF group at a distance of 0–25 μm as well as for the distance of 30–50 μm (0.004 ± 0.001 NIC, 0.005 ± 0.001 NIC, $p=0.017$; 0.004 ± 0.001 NIC, 0.005 ± 0.001 NIC, $p=0.019$). No significant difference in P signal after 50 μm was observed (0.004 ± 0.001 NIC vs. 0.006 ± 0.001 NIC, $p=0.107$) (Fig. 4f).

Spectral information

Further spectral information of the additional specimen per group (total, CTL $n=4$; FF $n=5$) was obtained by applying the same selection criteria as described earlier for XPS. This was done to allow comparison of NIC for Ca and P from different patients between FF and CTL groups. The results are shown in Fig. 3d, e and summarized in Table 2. The NIC for Ca and P ions are consistent with the XPS results, showing a significant decrease in P NIC for the FF group compared to the CTL group (Fig. 3e, Table 2). The mean Ca NIC were not significantly different between the two study groups (in accordance with the XPS data), although they showed a trend towards a higher amount of Ca in the FF group (Fig. 3d, Table 2).

BSEM

The Gaussian curve of the Ca distribution, giving information about the bone mineralization density distribution was calculated from ten randomly acquired BSEM images per bone sample representing the group mean weight percent Ca (Fig. 5, Table 2). The mean weight percent was not significantly different between the groups ($p=0.18$). The full width at half maximum (FWHM) of the histogram of the Ca distribution was slightly lower in the FF group when compared to CTL, indicated by a narrower curve ($p=0.10$) (Fig. 5, Table 2). This suggests a trend towards lower

heterogeneity of mineralization in the FF group. However, none of the BSEM outcomes showed statistically significant differences between FF and CTL.

Discussion

We used complementary surface analytical techniques to study human bone material properties of the femoral head in male patients with fragility fractures and male age-matched non-fracture controls. Recently, the problem of osteoporosis and the related fragility fractures in men has been recognized as an important public health issue and investigations are needed to determine factors contributing to bone quality/bone strength to enable the prediction of fracture risk. Bone strength is derived from bone quantity (BV/TV) and bone quality, which includes bone structure (micro- and macroarchitecture) and material properties, all primarily governed by bone turnover [8]. Although BMD measurements are widely available and a noninvasive way to identify postmenopausal individuals with osteoporosis and, possibly, those at high risk for fracture, the literature emphasizes the importance of bone quality when estimating fracture risk, especially in the male population [25–27]. In cases where BV/TV and BMD do not give satisfactory fracture risk estimations, additional Ca/P investigations may enable a better understanding of the quality of bone.

BMDD measured via BSEM indirectly reflects the mean tissue age of the bone, which in itself is determined by the rate of remodeling manifested as BSU with different degrees of mineralization [6, 28, 29] and a healthy individual usually does not exhibit a uniform level of mineralization because each basic BSU is at a different point in the remodeling cycle [6, 30]. Although the effect of increased homogeneity of bone tissue is unclear, the general principles of fracture mechanics suggest that homogeneity will impair fracture toughness and make brittle fracture more likely. Busse et al. compared bone from fragility fractures with bone from non-fracture controls revealing higher mineralized zones framed by lower mineralized trabecular surfaces in intact trabeculae, resulting in a beneficial composition supporting bone stability and toughness [31]. The BSEM examinations showed no significant differences in the mean weight percent of Ca between the groups. However, a more homogeneous mineralization, characterized by the narrow shape of the BMDD curve, expressed as the FWHM in the FF group was observed. Previous BSEM studies compared osteoporosis, osteoarthritis and the resulting effects of treatment [21, 26, 27, 32, 33] and showed that the allocation of BMDD is altered in osteoporotic male patients with high bone turnover when compared to BMDD of healthy individuals [6, 34–36] leading to the hypothesis that the increase in mineralization

seen in the investigated patients of the current study may be a normal response to maintain bone strength. In contrast to our results, the study of Fratzi-Zelman et al. associated fragility fractures in men with undermineralization and increased heterogeneity of the bone matrix without evidence of increased bone turnover [37]. This may be due to the significantly lower and wider age range (18–61 years) or may be a normal response to the various fractures at different skeletal sites reported from the participants of this study cohort, both of which may result in altered mineralization kinetics. The literature is contradictory and other recent studies have shown associated increased fracture risk with increased bone heterogeneity [31, 38, 39]. Further studies are clearly needed to improve our understanding of the role for the distribution of mineralization in bone fragility for a given patient and to understand the marked inter-individual variability of the distribution of mineralization within the osteoporotic population.

Currently, only the amount of Ca, as a part of HA, the main building block of bone's mineral, is considered in BMD measurements and not the quality of the mineralized bone matrix. P is one of the important components of HA and our results showed a significant decrease in P levels associated with fragility fracture. The alterations found in the spatial distribution, the amounts and ratios of Ca and P are likely to influence bone quality, with an imbalance towards P related to fragility fractures. Traditional investigations of Ca and P require ashing of the bone specimen, necessitating the destruction of the bone prior to analysis thus preventing microstructural quantitative analysis of different mineralization stages.

Histomorphometry and quantitative histology of iliac crest biopsies have greatly enhanced our understanding of normal bone microstructure, remodeling and strength, as well as the effects on bone of various diseases and treatments for osteoporosis and are widely used methods to assess bone diseases [40]. Histomorphometric findings in osteoporotic bone typically include reduced BV/TV, low trabecular number, impaired trabecular thickness as well as poor connectivity with increased trabecular separation. However, histomorphometry is invasive, and thus longitudinal measurements of bone structure at the same location are difficult to follow-up.

Recent data suggest that changes in blood serum bone turnover markers may be an accurate and non-invasive predictor of fracture risk reduction, but methods to measure bone turnover markers still suffer inter- and intra-specimen accuracy and sensitivity to be widely applied for fracture risk estimations. Our data may indicate alterations of bone turnover due to differences found in the diameter of BSUs as measured via XPS imaging considering how the diameter of BSUs is sensitive to the balance between resorption and formation of bone. Bone remodeling

requires the sequential and coordinated actions of the osteoclasts to remove bone and the osteoblasts to replace it. A change in this balance ultimately results in altered new bone deposition and subsequent mineralization as reflected in a change in BSU diameter.

Bone turnover also depends on osteocytes. Osteocytes account for more than 90% of all bone cells and are found scattered throughout the mineralized matrix. Osteocytes express several factors known to regulate phosphate metabolism, which suggests a role in matrix mineralization. Osteocytes sense bone deformation, thereby signaling the need for adaptive remodeling of bone size, shape and distribution to accommodate prevailing loads which may be seen as differences in P distribution as measured via XPS and TOF-SIMS. The FF group did not show an accumulation at certain areas in the distribution of P, whereas in the CTL group, patches of P are clearly visible, which is in agreement with the characterization of osteoporotic bone being in a state of altered bone turnover [41]. The fact that the FF group exhibited significant differences also in the amount of P present in the newly formed bone areas suggests that in trabecular bone of FF patients, not only the amount of the newly formed bone areas is reduced (diameter of the BSU), but the quality of this freshly deposited bone matrix also seems to be altered.

Hirschman et al. investigated *in vitro* cartilage calcification in rats and reported a lower Ca/P ratio in young growing bone (areas of new calcification) when compared to older, higher mineralized bone areas. This finding is in agreement with the here presented results of the CTL group exhibiting significantly lower Ca/P ratio in the CaLOW when compared to CaHIGH areas [42]. Previous studies on Ca and P concentrations and Ca/P ratio in osteoporosis are conflicting [43]. Studies from Basle et al. compared Ca/P ratio via energy dispersive X-ray microanalysis investigating a comparable number of male CTL and OP ($n=4:6$) and showed no differences in Ca and P concentration in cortical and trabecular bone [43] which may be due to the fact that only higher mineralized areas (excluding haversian canals, cortical lacunae and trabecular surfaces) were analyzed. Those areas did not show differences in our investigations either. It is well accepted that changes in bone mass in males leading to osteoporosis are due to a climacteric rather than aging factors. Such changes in bone mass are expected after the age of 50 caused by the suppression of bone turnover [44]. The very wide age range (31–87 years of age) used in the study from Basle et al. might explain the observed lack of differences, whereas the age range of the study presented here ensured a similar state of bone turnover (65–80 years of age) and exhibited therefore more distinct differences.

Previous observations in ashed human bone biopsies also revealed no age-related difference in mineral content

[45] or in Ca and P concentration in trabecular bone [46] which leads us to conclude that the intra-specimen investigation of lower mineralized areas vs. higher mineralized areas is of crucial importance. Given the absence of BMD measurements and bone turnover status, we are reluctant to overemphasize the clinical relevance of our findings. But we do observe a significant differential in Ca and P in the male FF specimens investigated.

Our data are in agreement with recent publications indicating the importance of material properties as a contributor to bone strength [47], leading to the conclusion that the underlying mechanism lies in bone quality, investigated here as the interrelationship of Ca and P. Although this study has several limitations, such as small sample size, sampling location limited to one skeletal site (femoral head), the lack of detailed patient information and bone status with regards to tissue age, the increasing acceptance of bone quality parameters [8] as contributing factors affecting bone mechanical strength makes the parameter of Ca/P ratio a potential clinical tool [46, 48]. Nonetheless, further investigations and large scale intervention studies are needed to elucidate the material factors, such as the here investigated ratio of Ca and P, negatively influencing bone quality. This is an especially exciting prospect since *in vivo* measurement of bone Ca/P ratio [10] in humans could in the future be possible, since it is already being successfully applied on animals [48].

Conclusions

A novel and distinguishing characteristic of the present study is the use of a combination of complementary imaging spectroscopic and microscopic techniques enabling insights into both the micro- and nanoscale spatial distribution and the relationship of Ca and P. We used XPS and TOF-SIMS to assess the interrelationship between Ca and P as a potential indicator of the quality of mineralization in human femoral bone from male patients with fragility fractures. The inclusion of spatial distribution of both Ca and P on trabecular bone may hold the key to better and more comprehensive fracture risk assessment as an addition to the well-established BMD measurements. The results provide evidence that the Ca/P ratio of bone could be a valuable parameter to be used during bone therapeutic and diagnostic trials. In addition, the present study, although it is a biological bone study rather than a clinical study for immediate application to patients, may be useful for follow-up studies in the diagnosis or treatment of skeletal disorders.

Acknowledgements The authors would like to thank the staff of the Department of Orthopaedics and Trauma in the Royal Adelaide

Hospital and the mortuary staff of SA Pathology, Adelaide for the collection of femoral and autopsy specimens. Furthermore, the authors acknowledge the facilities and scientific and technical assistance of the Australian Microscopy & Microanalysis Research Facility. This work was supported by a grant from the Australian Research Council (DP0878419).

Conflicts of interest None.

References

- Rachner TD, Khosla S, Hofbauer LC (2011) Osteoporosis: now and the future. *Lancet* 377:1276–1287
- Chavassieux P, Seeman E, Delmas PD (2007) Insights into material and structural basis of bone fragility from diseases associated with fractures: how determinants of the biomechanical properties of bone are compromised by disease. *Endocr Rev* 28:151–164
- Schuit SCE, van der Klift M, Weel AEAM, de Laet CEDH, Burger H, Seeman E, Hofman A, Uitterlinden AG, van Leeuwen JPTM, Pols HAP (2004) Fracture incidence and association with bone mineral density in elderly men and women: the Rotterdam study. *Bone* 34:195–202
- Zulc P, Munoz F, Duboeuf F, Marchand F, Delmas PD (2005) Bone mineral density predicts osteoporotic fractures in elderly men: the MINOS study. *Osteoporos Int* 16:1184–1192
- Fratzl P, Gupta HS, Paschalis EP, Roschger P (2004) Structure and mechanical quality of the collagen-mineral nano-composite in bone. *J Mater Chem* 14:2115–2123
- Roschger P, Gupta HS, Berzlanovich A, Ittner G, Dempster DW, Fratzl P, Cosman F, Parisien M, Lindsay R, Nieves JW, Klaushofer K (2003) Constant mineralization density distribution in cancellous human bone. *Bone* 32:316–323
- Faibish D, Ott SM, Boskey AL (2006) Mineral changes in osteoporosis: a review. *Clin Orthop Relat Res* 443:28–38
- Felsenberg D, Boonen S (2005) The bone quality framework: determinants of bone strength and their interrelationships, and implications for osteoporosis management. *Clin Ther* 27:1–11
- Shapiro R, Heaney RP (2003) Co-dependence of calcium and phosphorus for growth and bone development under conditions of varying deficiency. *Bone* 32:532–540
- Fountos G, Yasumura S, Glaros D (1997) The skeletal calcium/phosphorus ratio: a new in vivo method of determination. *Med Phys* 24:1303–1310
- Tzaphlidou M, Speller R, Royle G, Griffiths J, Olivo A, Pani S, Longo R (2005) High resolution Ca/P maps of bone architecture in 3D synchrotron radiation microtomographic images. *Appl Radiat Isot* 62:569–575
- Eriksson C, Börner K, Nygren H, Ohlson K, Bexell U, Billerdaahl N, Johansson aM (2006) Studies by imaging TOF-SIMS of bone mineralization on porous titanium implants after 1 week in bone. Proceedings of the fifteenth international conference on secondary ion mass spectrometry, 30 July 2006. -SIMS XV, Applied Surface Science, volume 252, issue 19, pp 6757–6760
- Belu AM, Graham DJ, Castner DG (2003) Time-of-flight secondary ion mass spectrometry: techniques and applications for the characterization of biomaterial surfaces. *Biomaterials* 24:3635–3653
- Malmberg P, Nygren H (2008) Methods for the analysis of the composition of bone tissue, with a focus on imaging mass spectrometry (TOF-SIMS). *Proteomics* 8:3755–3762
- deVries J (1998) Surface characterization methods—XPS, TOF-SIMS, and SAM a complimentary ensemble of tools. *J Mater Eng Perform* 7:303–311
- Boivin G, Meunier PJ (2004) Inter-individual heterogeneity index of mineralization is an important determinant of the quality of bone. *J Bone Miner Res* 19:S114–S114
- Boivin G, Farlay D, Bala Y, Doublier A, Meunier PJ, Delmas PD (2009) Influence of remodeling on the mineralization of bone tissue. *Osteoporos Int* 20:1023–1026
- Boivin G, Meunier PJ (2003) The mineralization of bone tissue: a forgotten dimension in osteoporosis research. *Osteoporos Int* 14:S19–S24
- Shirley DA (1972) High-resolution X-ray photoemission spectrum of the valence bands of gold. *Phys Rev B* 5:4709–4714
- Jung S, Foston M, Sullards MC, Ragauskas AJ (2010) Surface characterization of dilute acid pretreated populus deltoides by TOF-SIMS. *Energ Fuel* 24:1347–1357
- Zoehrer R, Roschger P, Paschalis EP, Hofstaetter JG, Durchschlag E, Fratzl P, Phipps R, Klaushofer K (2006) Effects of 3- and 5-year treatment with risedronate on bone mineralization density distribution in triple biopsies of the iliac crest in postmenopausal women. *J Bone Miner Res* 21:1106–1112
- Vickerman J, Briggs D, SurfaceSpectra (2001) ToF-SIMS: surface analysis by mass spectrometry. Chichester: IM, Manchester
- Sutton-Smith P, Beard H, Fazzalari N (2008) Quantitative back-scattered electron imaging of bone in proximal femur fragility fracture and medical illness. *J Microsc* 229:60–66
- Roschger P, Fratzl P, Eschberger J, Klaushofer K (1998) Validation of quantitative backscattered electron imaging for the measurement of mineral density distribution in human bone biopsies. *Bone* 23:319–326
- Ruppel ME, Miller LM, Burr DB (2008) The effect of the microscopic and nanoscale structure on bone fragility. *Osteoporos Int* 19:1251–1265
- Vashishth D, Merle B, Gineyts E, Boivin G, Allen M, Burr DB, Delmas PD (2007) Effects of alendronate-induced bone matrix changes on resorption and turnover. *J Bone Miner Res* 22:S445–S445
- Doublier A, Farla D, Khebbab MT, Jaurand X, Meunier PJ, Boivin G (2010) Bone mineral quality is maintained in osteoporotic women treated up to 60 months with strontium ranelate. *Osteoporos Int* 21:22–22
- Boivin G, Meunier PJ (2002) The degree of mineralization of bone tissue measured by computerized quantitative contact microradiography. *Calcif Tissue Int* 70:503–511
- Boivin G, Meunier PJ (2002) Changes in bone remodeling rate influence the degree of mineralization of bone. *Connect Tissue Res* 43:535–537
- Loveridge N, Power J, Reeve J, Boyde A (2004) Bone mineralization density and femoral neck fragility. *Bone* 35:929–941
- Busse B, Hahn M, Soltau M, Zustin J, Puschel K, Duda GN, Amling M (2009) Increased calcium content and inhomogeneity of mineralization render bone toughness in osteoporosis: mineralization, morphology and biomechanics of human single trabeculae. *Bone* 45:1034–1043
- Boivin G, Farlay D, Khebbab MT, Jaurand X, Delmas PD, Meunier PJ (2010) In osteoporotic women treated with strontium ranelate, strontium is located in bone formed during treatment with a maintained degree of mineralization. *Osteoporos Int* 21:667–677
- Bala Y, Chapurlat R, Delmas PD, Boivin G (2009) There is no hypermineralization among postmenopausal women receiving long-term oral bisphosphonates. *Osteoporos Int* 20:68–68
- Roschger P, Paschalis EP, Fratzl P, Klaushofer K (2008) Bone mineralization density distribution in health and disease. *Bone* 42:456–466
- Peterlik H, Roschger P, Klaushofer K, Fratzl P (2006) From brittle to ductile fracture of bone. *Nat Mater* 5:52–55
- Fratzl-Zelman N, Roschger P, Gourrier A, Weber M, Misof BM, Loveridge N, Reeve J, Klaushofer K, Fratzl P (2009) Combination

- of nanoindentation and quantitative backscattered electron imaging revealed altered bone material properties associated with femoral neck fragility. *Calcif Tissue Int* 85:335–343
37. Fratzl-Zelman N, Roschger P, Misof BM, Nawrot-Wawrzyniak K, Potter-Lang S, Muschitz C, Resch H, Klaushofer K, Zwettler E (2011) Fragility fractures in men with idiopathic osteoporosis are associated with undermineralization of the bone matrix without evidence of increased bone turnover. *Calcif Tissue Int* 88:378–387
 38. Bousson V, Bergot C, Wu Y, Jolivet E, Zhou L, Laredo J-D (2011) Greater tissue mineralization heterogeneity in femoral neck cortex from hip-fractured females than controls. A microradiographic study. *Bone* 48:1252–1259
 39. Dong XN, Luo Q, Sparkman DM, Millwater HR, Wang X (2010) Random field assessment of nanoscopic inhomogeneity of bone. *Bone* 47:1080–1084
 40. Rizzoli R (2010) Microarchitecture in focus. *Osteoporos Int* 21:403–406
 41. Seeman E, Delmas PD (2006) Mechanisms of disease—bone quality—the material and structural basis of bone strength and fragility. *New Engl J Med* 354:2250–2261
 42. Hirschman A, Sobel AE (1965) Composition of the mineral deposited during in vitro calcification in relation to fluid phase. *Arch Biochem Biophys* 110:237–243
 43. Basle MF, Mauras Y, Audran M, Clochon P, Rebel A, Allain P (1990) Concentration of bone elements in osteoporosis. *J Bone Miner Res* 5:41–47
 44. Goderie-Plomp HW, van der Klift M, de Ronde W, Hofman A, de Jong FH, Pols HAP (2004) Endogenous sex hormones, sex hormone-binding globulin, and the risk of incident vertebral fractures in elderly men and women: the Rotterdam study. *J Clin Endocrinol Metab* 89:3261–3269
 45. Roschger P, Fratzl P, Eschberger J (1998) Validation of quantitative backscattered electron imaging for the measurement of mineral density distribution in human bone biopsies. *Bone* 23:319–326
 46. Zaichick V, Tzaphlidou M (2003) Calcium and phosphorus concentrations and the calcium/phosphorus ratio in trabecular bone from the femoral neck of healthy humans as determined by neutron activation analysis. *Appl Radiat Isot* 58:623–627
 47. Boyde A, Jones SJ, Aerssens J, Dequeker J (1995) Mineral density quantitation of the human cortical iliac crest by back-scattered electron image analysis: variations with age, sex, and degree of osteoarthritis. *Bone* 16:619–627
 48. Tzaphlidou M, Speller R, Royle G, Griffiths J, Olivo A, Pani S, Longo R (2005) High resolution Ca/P maps of bone architecture in 3D synchrotron radiation microtomographic images. *Appl Radiat Isot* 62:569–575